


Transport properties of ultrathin $\text{BaFe}_{1.84}\text{Co}_{0.16}\text{As}_2$ superconducting nanowires

Pusheng Yuan^{1,2,3} , Zhongtang Xu¹, Chen Li¹, Baogang Quan⁴, Junjie Li⁴, Changzhi Gu⁴ and Yanwei Ma^{1,3}

¹ Key Laboratory of Applied Superconductivity, Institute of Electrical Engineering, Chinese Academy of Sciences, Beijing 100190, People's Republic of China

² Shanghai Institute of Microsystem and Information Technology, Chinese Academy of Sciences, 865 Changning Road, Shanghai 200050, People's Republic of China

³ University of Chinese Academy of Sciences, Beijing 100049, People's Republic of China

⁴ Beijing National Laboratory for Condensed Matter Physics, Institute of Physics, Chinese Academy of Sciences, Beijing 100190, People's Republic of China

E-mail: ywma@mail.iee.ac.cn

Received 30 August 2017, revised 15 November 2017

Accepted for publication 17 November 2017

Published 19 December 2017



Abstract

Superconducting nanowire single-photon detectors (SNSPDs) have an absolute advantage over other types of single-photon detectors, except for the low operating temperature. Therefore, much effort has been devoted to finding high-temperature superconducting materials that are suitable for preparing SNSPDs. Copper-based and MgB_2 ultrathin superconducting nanowires have already been reported. However, the transport properties of iron-based ultrathin superconducting nanowires have not been studied. In this work, a 10 nm thick \times 200 nm wide \times 30 μm long high-quality superconducting nanowire was fabricated from ultrathin $\text{BaFe}_{1.84}\text{Co}_{0.16}\text{As}_2$ films by a lift-off process. The precursor $\text{BaFe}_{1.84}\text{Co}_{0.16}\text{As}_2$ film with a thickness of 10 nm and root-mean-square roughness of 1 nm was grown on CaF_2 substrates by pulsed laser deposition. The nanowire shows a high superconducting critical temperature $T_c^{\text{zero}} = 20$ K with a narrow transition width of $\Delta T = 2.5$ K and exhibits a high critical current density J_c of $1.8 \times 10^7 \text{ A cm}^{-2}$ at 10 K. These results of ultrathin $\text{BaFe}_{1.84}\text{Co}_{0.16}\text{As}_2$ nanowire will attract interest in electronic applications, including SNSPDs.

Keywords: nanowire, pulsed laser deposition, ultrathin film, iron-based superconductors, single-photon detectors

(Some figures may appear in colour only in the online journal)

Introduction

Superconducting nanowire single-photon detectors (SNSPDs) demonstrate a distinct advantage over other types of single-photon detectors, and have generated tremendous interest in the scientific community [1, 2]. Although SNSPDs have more advantages than other single-photon detectors such as avalanche photodiodes, one drawback is the low operating temperature because current SNSPDs are fabricated from conventional low-temperature superconductors (NbN, WSi). To increase the operating temperature, much effort has been

devoted to exploring suitable superconducting materials with high T_c for the preparation of SNSPDs includes MgB_2 and cuprate superconductors [3–8]. Iron-based superconductors, as one important member of the high-temperature superconducting materials, have attracted much effort to explore its application in the field of large-scale current transport [9, 10] and in micro-electronics or nano-electronics applications [11, 12]. However, the transport properties of ultrathin iron-based superconducting nanowires have not been studied because the critical temperature of iron-based superconducting film strongly depends on the thickness. Typically,

thinner films present worse superconductivity [13–15] (except for single-layer film [16]). For this reason, exploring iron-based superconducting film applications in the field of micro-electronics or nano-electronics only was limited to a relatively thick scale [17–19]. To our knowledge, there is no report on the transmission characteristics of Fe-based superconducting thin films with thickness less than 30 nm, because the 30 nm thick film shows a J_c one order of magnitude lower than the films with thickness more than 70 nm [13]. To explore a possible application of iron-based superconductors to SNSPDs, it is necessary to prepare high-quality ultrathin (about 10 nm) iron-based superconducting films. Among the iron-based superconductors, $\text{BaFe}_{2-x}\text{Co}_x\text{As}_2$ epitaxial films have been extensively investigated because of the higher critical transition temperature, better stability and easy growth by pulsed laser deposition (PLD) [20–22]. Therefore, $\text{BaFe}_{1.84}\text{Co}_{0.16}\text{As}_2$ (Ba122:Co) was selected to prepare high-quality ultrathin film and to explore the feasibility of Ba122:Co application in SNSPDs.

In this work, we report the first fabrication of superconducting nanowire from PLD-prepared Ba122:Co films 10 nm thick by micro-nanofabrication technologies. From the transport measurement, the obtained 200 nm wide $\text{BaFe}_{1.84}\text{Co}_{0.16}\text{As}_2$ nanowires show $T_c^{\text{zero}} = 20$ K, transition width $\Delta T = 2.5$ K, and exhibit a high critical current density J_c of $1.8 \times 10^7 \text{ A cm}^{-2}$ at 10 K, suggesting their potential in making iron-based SNSPDs with high operating temperatures.

Experimental details

Although MgO , $(\text{LaAl})_{0.7}(\text{SrAl}_{0.5}\text{Ta}_{0.5})_{0.3}\text{O}_3$ (LSAT), LaAlO_3 (LAO), SrTiO_3 (STO) and CaF_2 single-crystalline substrates are often used to prepare Ba122:Co superconducting films, high-performance superconducting films with thickness less than 30 nm have not yet been prepared [13, 21, 23]. These substrates were chosen and tried, to prepare high-quality ultrathin Ba122:Co films by PLD. The details of the growth conditions were reported in our previous work [24]. The substrates were cleaned in an ultrasonic bath by using alcohol and acetone for 5 min, respectively, and then the clean substrate was glued onto a stainless-steel sample holder by silver paint. The laser (KrF 248 nm) energy was chosen to be 310–320 mJ per pulse with a repetition rate of 9 Hz and the distance between the substrate and target was kept fixed at 40 mm. A base pressure of 10^{-7} Torr was maintained and increased to 10^{-6} Torr during the deposition due to degassing. The Ba122:Co films were prepared at 700 °C, and before the film deposition the target surface was cleaned by about 1000 laser pulses. The deposition pulse number was varied in the range of 800–12 000 and the corresponding thickness was 10–150 nm. After deposition, the film was cooled down to room temperature at a rate of $10^\circ\text{C min}^{-1}$. As the high-quality ultrathin Ba122:Co film was successfully prepared on CaF_2 substrate, in order to get superconducting nanowires, we developed a special nanofabrication procedure for our Ba122:Co film (as shown in figure 1). First, a thin film of Cr/Au was deposited on the

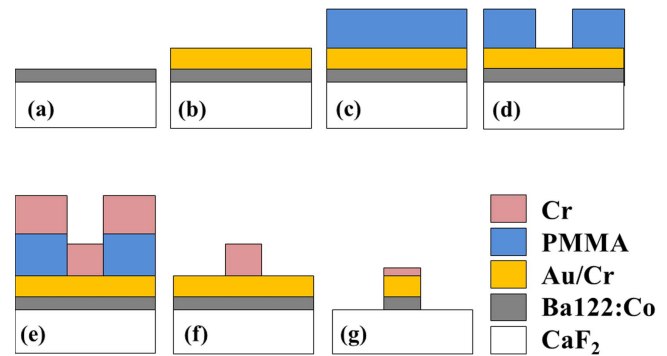


Figure 1. Schematic diagrams to illustrate the process of nanowire fabrication on ultrathin Ba122:Co films.

as-prepared Ba122:Co film by an electron-beam evaporation technique (figure 1(b)). The thicknesses of chromium and gold are 10 and 60 nm, respectively, which are adequate to protect the Ba122:Co film from moisture during subsequent processes. Then, a layer of PMMA electron-beam resist was applied by spin-coating (figure 1(c)). A 200 nm wide line was defined by electron-beam lithography in the PMMA resist (figure 1(d)). For optical alignment in the fabrication of the nanowire device, the length of the lines was defined as 30 μm . Thereafter, an electron-beam evaporation of 60 nm chromium film was conducted (figure 1(e)) and followed by a lift-off process to obtain a chromium line (figure 1(f)). Next, the pattern of the line was transferred to a multilayer film of Cr/Au on Ba122:Co to form Au/Cr/Ba122:Co nanowire (figure 1(g)) by Ar ion-beam etching. The reason for choosing Cr as the etching mask for the fabrication of superconducting nanowires is that the etching rate of Cr is much slower than that of gold in the Ar ion-beam etching process. And the 60 nm thickness of chromium can withstand the etching process of the Au/Cr/Ba122:Co multilayer. With the protection of the Cr/Au cover layer, our Ba122:Co nanowire becomes compatible with standard-device micro-fabrication processes. Finally, a 10 nm thick \times 200 nm wide \times 30 μm long Ba122:Co nanowire with four-electrode configuration was fabricated by photolithography, Cr (5 nm)/Au (60 nm) metallization and lift-off. If the light is incident on the nanowire, the current method of preparing nanowires may lead to a decrease in the performance of the SNSPD, which results in the incident photons being absorbed or reflected by the thick metallic multilayer on the nanowires. This way of irradiating nanowires with back incident is often adopted by SNSPD. Fortunately, the substrate CaF_2 of Ba122:Co nanowires have a high optical transmittance. To avoid the absorption and reflection of the thick metallic multilayer when the incident is normal, we can irradiate the nanowires from the backside with light passing through the substrate CaF_2 . In addition, we can also try other processes that may be more suitable for preparing single-photon detectors, as reported in [25]. A scanning electron microscope (SEM) and atomic force microscope (AFM) were used to obtain the microstructure and the surface topography of the samples, respectively. The transport properties of the Ba122:Co films

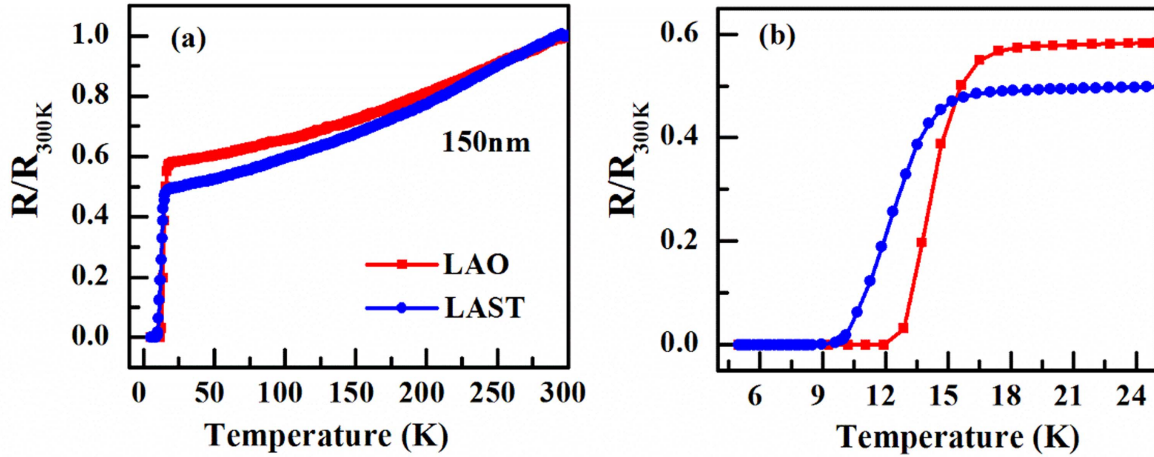


Figure 2. (a) Resistance versus temperature of Ba122:Co films on LSAT and LAO substrates. (b) Detail of superconducting transition for Ba122:Co films on LSAT and LAO substrates. Resistance has been normalized to the value of $R(300\text{ K})$.

and nanowires were measured in four-probe configuration with a physical property measurement system.

Results and discussion

The thermal relaxation capacity of SNSPD depends on the heat capacity and heat transfer between the film and substrate [26]. If we only consider the impact of heat capacity on the thermal relaxation capacity, thinner film generally exhibits faster thermal relaxation. The specific heat capacity of Ba122:Co [27] is larger than MgB_2 [28]; therefore, the same thermal relaxation capacity requires Ba122:Co to be thinner relative to MgB_2 film (usually about 10 nm or less than 10 nm in thickness). In order to prepare iron-based superconducting thin film suitable for SNSPDs, Ba122:Co films with various thickness were grown on different single-crystalline substrates by PLD. First, the 150 nm thick Ba122:Co films were deposited on the LSAT and LAO substrates. Figure 2 shows the temperature dependence of resistivity for Ba122:Co films. The critical temperatures of the films on the LSAT and LAO substrates were $T_c^{\text{onset}} = 16\text{ K}$ and $T_c^{\text{onset}} = 14\text{ K}$, respectively. These values are much lower than the critical transition temperature of the Ba122:Co target ($T_c^{\text{onset}} = 26\text{ K}$). Moreover, previous reports point out that thinner film tends to induce lower critical transition temperature [13]. Therefore, LSAT and LAO substrates are not suitable for the preparation of ultrathin Ba122:Co superconducting films. Soon after, Ba122:Co films were grown on MgO and STO substrates. Figure 3 shows resistance versus temperature (R - T) curves normalized by resistance at 300 K ($R(300\text{ K})$) for thin films with different thickness from 10–187 nm. It can be seen that, with the same film thickness, the critical transition temperature of Ba122:Co thin films grown on MgO and STO substrates is superior to those grown on LSAT and LAO substrates. At the same time, there is striking evidence that the film thickness strongly affects the critical transition temperature. As shown in figures 3(a) and (b), the critical transition temperature of 150 nm thick Ba122:Co films grown on MgO

substrates was $T_c^{\text{onset}} = 20\text{ K}$. Unfortunately, complete superconductivity transition was not observed in the film with a thickness below 37.5 nm even if the test temperature is reduced to 5 K. As can be seen from figures 3(c) and (d), the critical transition temperature of Ba122:Co film grown on the STO substrate was higher than the film on the MgO substrate. However, complete superconducting transition was not observed down to 5 K for film with a thickness of 10 nm. The above results indicate that Ba122:Co films grown on MgO substrate and STO substrates are unable to meet the requirements of the SNSPDs. Fortunately, iron-based superconducting films grown on CaF_2 substrates tend to exhibit excellent superconducting properties [23, 29–33]. Thus, the CaF_2 substrate was chosen to grow ultrathin Ba122:Co films. It is exciting that the Ba122:Co films on the CaF_2 substrates not only have high superconducting transition temperature and narrow transition width but show superconductivity in films with thickness much less than those fabricated on other substrates. As shown in figures 4(a) and (b), as the thickness of the Ba122:Co film was reduced from 150 to 10 nm, the critical transition temperature T_c^{onset} decreased from 25.5 to 23.5 K and T_c^{zero} decreased from 23 to 20.8 K. For the same thickness, the critical temperature of Ba122:Co film depends strongly on the substrates. The highest T_c^{zero} and the lowest T_c^{zero} for the Ba122:Co films were on CaF_2 and LSAT substrates, respectively. The effect of the substrate on the critical transition temperature of the Ba122:Co film is consistent with the previous report [34]. Therefore, the 10 nm thick Ba122:Co thin film grown on CaF_2 substrate is suitable for exploring its application in the SNSPD field in terms of film thickness and superconducting transition temperature required by SNSPDs.

The superconducting films used to prepare high-performance SNSPDs require not only a sufficiently thin thickness but extremely low surface roughness. In order to investigate the surface morphology and surface roughness of Ba122:Co thin films, AFM studies were performed. Figure 5(a) shows a 12.5 nm thick Ba122:Co film with a step on the CaF_2 substrate. The AFM image was clearly divided into the left and right part, which are the surface topography of the CaF_2 substrate and Ba122:Co film, respectively. The surface

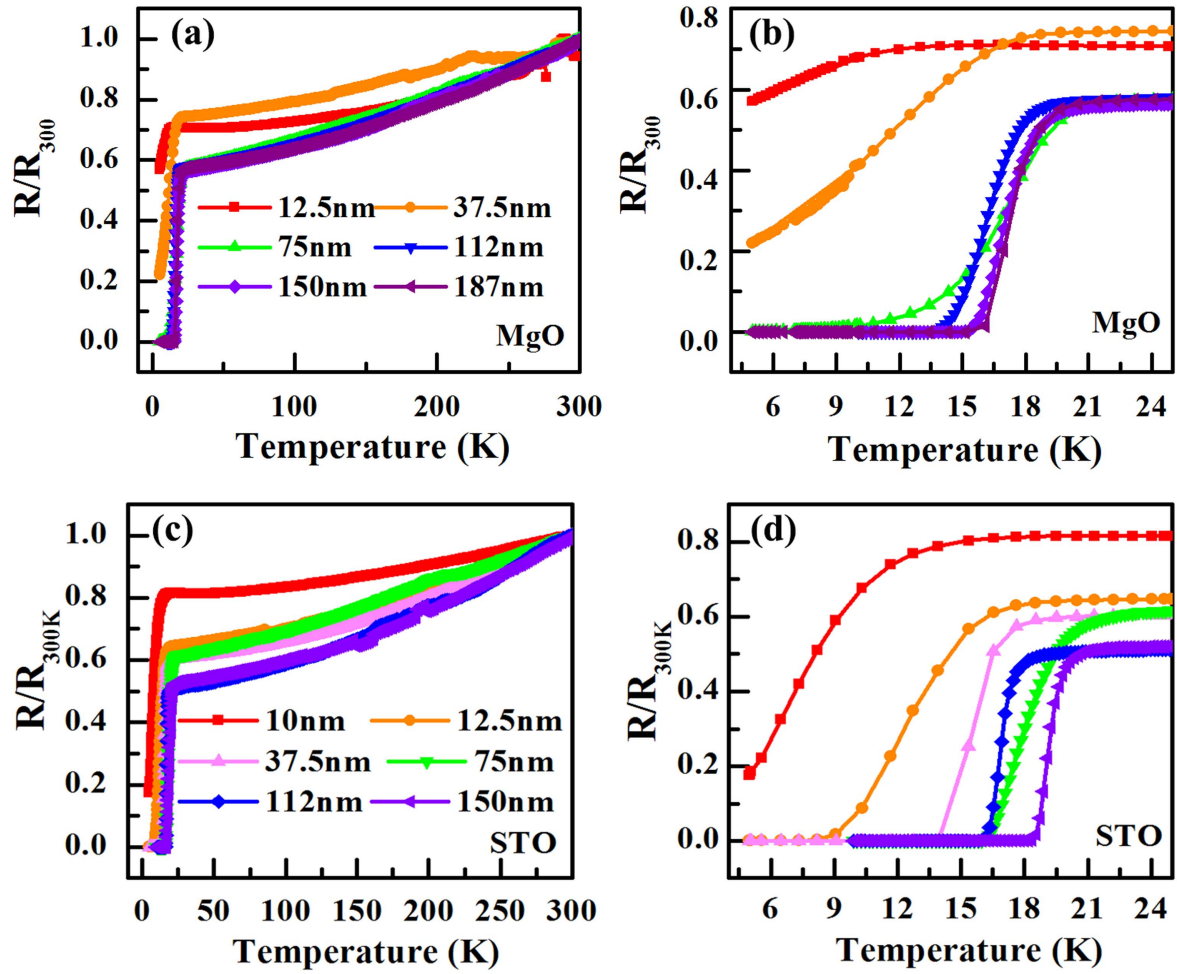


Figure 3. (a) and (c) show the resistance versus temperature of Ba122:Co films on MgO and STO substrates, respectively. (b) and (d) the detail of superconducting transition of Ba122:Co films on MgO and STO substrates, respectively. Resistance has been normalized to the value of $R(300\text{ K})$.

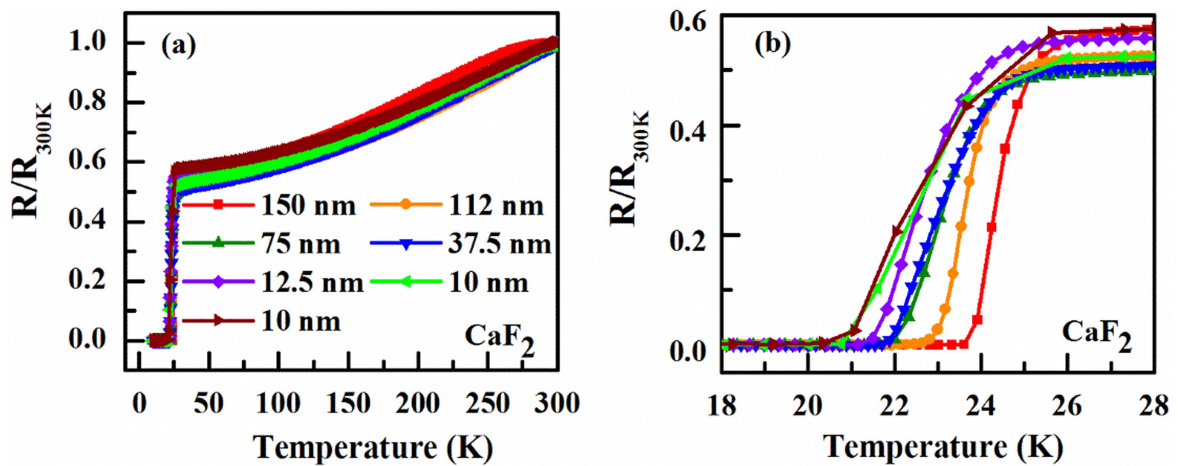


Figure 4. (a) Resistance versus temperature of Ba122:Co films on CaF_2 substrates. (b) Detail of superconducting transition for Ba122:Co films on CaF_2 substrates. Resistance has been normalized to the value of $R(300\text{ K})$.

topography of the film shows more or less round island shapes, not as smooth as the CaF_2 substrate. As shown in figure 5(b), the 10 nm thick Ba122:Co film also exhibits the same surface topography as that of the 12.5 nm thick film. The root-mean-square roughness of the Ba122:Co film in a

$12\text{ }\mu\text{m} \times 12\text{ }\mu\text{m}$ region is 1.05 nm. Figures 5(c) and (d) exhibit the SEM images of a $200\text{ nm wide} \times 30\text{ }\mu\text{m long}$ nanowire prepared by a 10 nm thick Ba122:Co film, which indicates that the electrodes are in full contact with the nanowire and the nanowire is uniform in width.

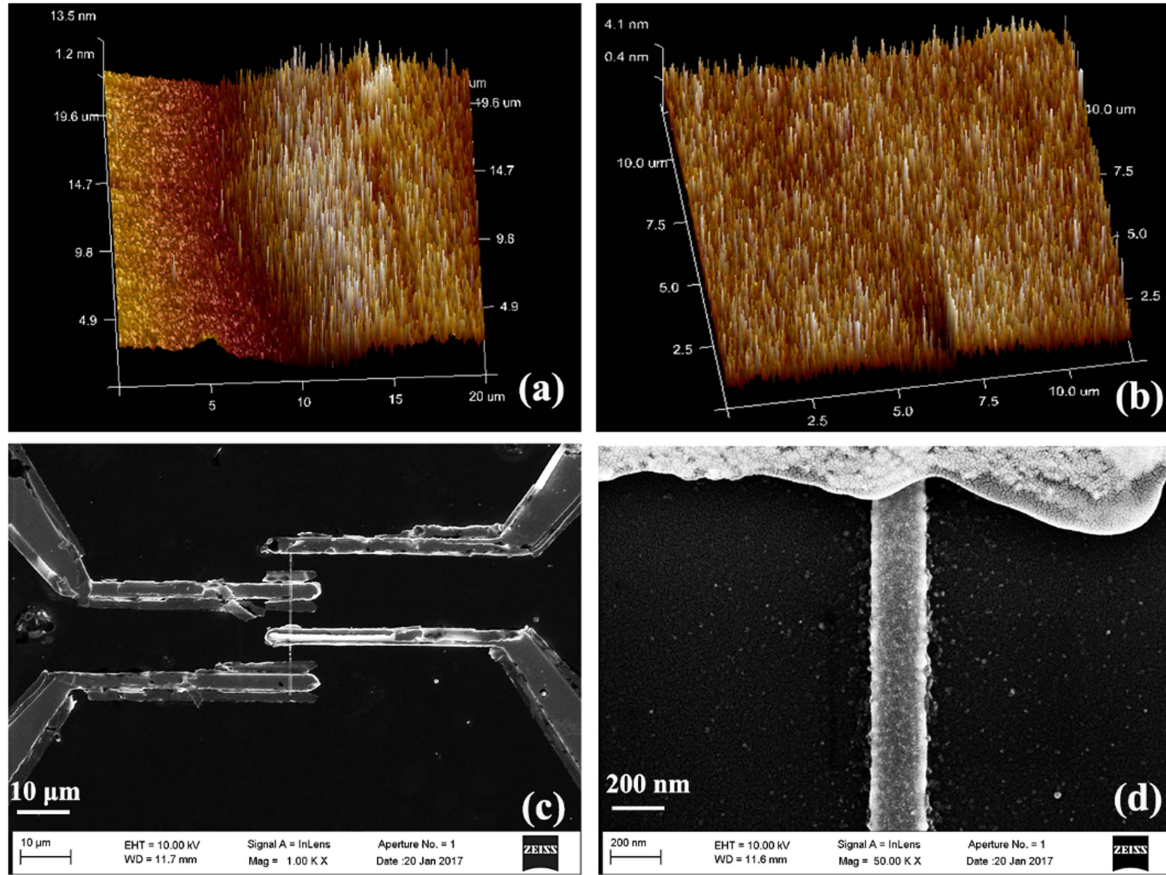


Figure 5. (a) AFM images of the CaF₂ substrate and 12.5 nm thick Ba122:Co film. (b) AFM images of the 10 nm thick Ba122:Co film with root-mean-square roughness 1.05 nm in a 12 μm × 12 μm region. (c) SEM image of a 10 nm thick × 200 nm wide × 30 μm long Ba122:Co nanowire. (d) Enlarged view of the Ba122:Co nanowire.

In order to check the influence of the micro-nanogrid process on the superconductivity of Ba122:Co nanowire, the superconducting transition of the nanowire had been compared with that of the Ba122:Co film in figure 6(a). The Ba122:Co film shows a sharp superconducting transition at 23.6 K (T_c^{onset}) with a narrow transition width of 2.2 K (ΔT_c). Compared with the film, the nanowire shows a slightly broader transition width $\Delta T_c = 2.5$ K and a decrease in T_c^{onset} of only about 1.1 K. It can be concluded that Ba122:Co nanowire and film display nearly the same superconducting transition temperature. Therefore, the method used in this study to process the Ba122:Co film into nanowire is appropriate. Figure 6(b) exhibits the R-T of the Ba122:Co nanowire for different test currents. The nanowire exhibits a superconducting transition temperature of $T_c^{\text{onset}} = 22.5$ K with a narrow transition width of 2.5 K at a measured current of 0.01 mA. As the measured current rises to 0.1 mA, the nanowire exhibits the same superconducting transition as in the situation of 0.01 mA, but the transition width ΔT_c increases from 2.5 to 5 K. This result indicates that the test current strongly affects the transition width of the nanowires. In general, the superconducting transition width of the superconducting material has a significant broadening in the magnetic field. Therefore, we suspect that the increase in the test current will result in the self-field enhancement of

the Ba122:Co nanowire, which further affects the increase in ΔT_c .

To further characterize the transport properties of the Ba122:Co nanowire, the I - V measurements were performed to determine the critical current (I_c) and the critical current density (J_c) as a function of temperature. Figure 6(c) shows the I - V characteristics of the Ba122:Co nanowire at selected temperatures. As can be seen, the resistive state of I - V characteristics emerges at each test temperature, and at small bias current densities, this phenomenon is the same as FeSe_{0.5}Te_{0.5} superconducting nanowire (500 and 800 nm) [35], but different from Ba122:Co micrometer-sized bridges (2.9, 3.5 and 4.7 μm) [17]. As Nappi *et al* reported, the resistive state emerging at low currents in the I - V test is due to the depinning (creep flow) of a very limited number of magnetic field lines [35]. Here, the critical current I_c has been defined as the current at which the voltage reaches the value $V = 50$ μV across the Ba122:Co nanowire, because the value of the voltage will increase dramatically and I - V curves show normal resistance state as it is larger than 50 μV. At 10 K, the I_c of nanowire was 0.36 mA, which corresponds to a large $J_c = 1.8 \times 10^7$ A cm⁻². The J_c value of Ba122:Co nanowire was comparable to that of La_{1.85}Sr_{0.15}CuO₄ and MgB₂ nanowire [4, 36] at 10 K. At the raised test temperature, the J_c of nanowire decreases gradually as shown in figure 6(d). At

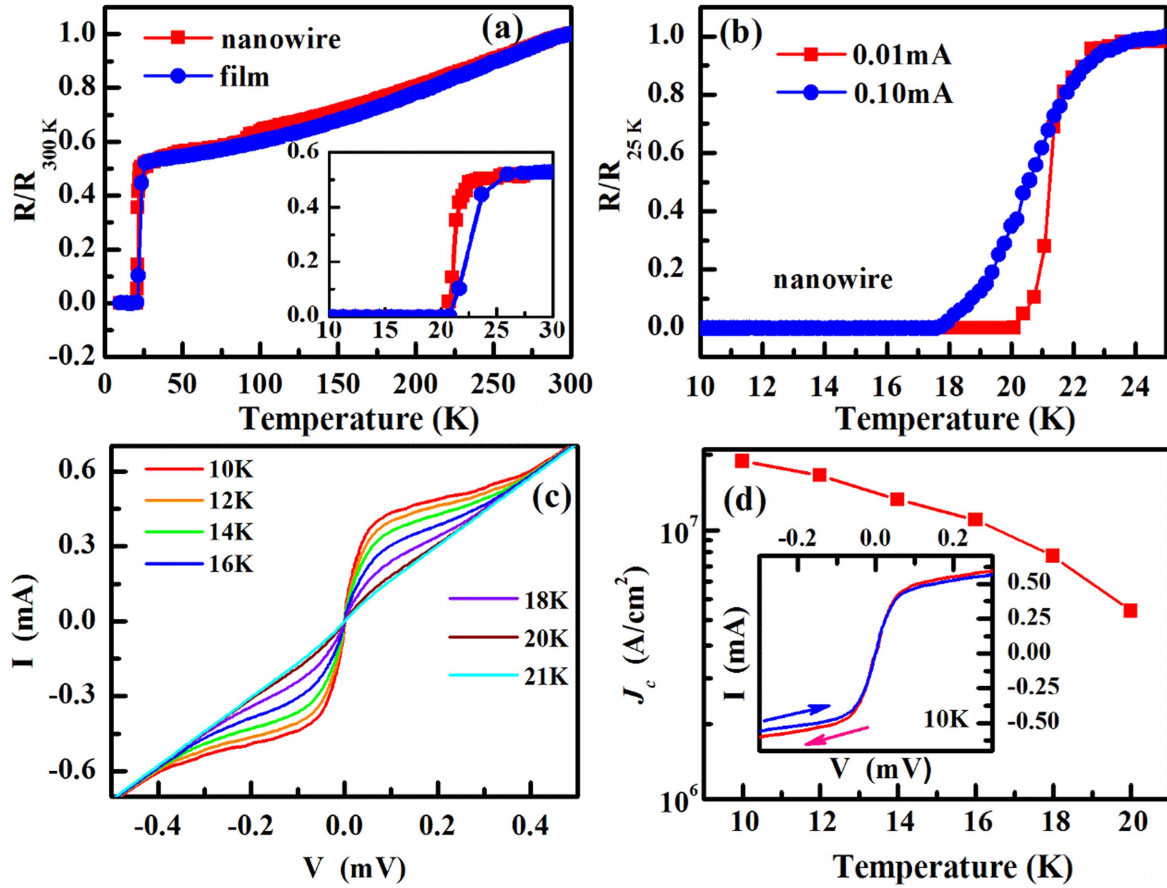


Figure 6. (a) Resistance versus temperature of the 10 nm thick Ba122:Co films and 200 nm wide Ba122:Co nanowire. Inset: detail of superconducting transition for the Ba122:Co film and nanowire. (b) Detail of superconducting transition for the Ba122:Co nanowire under different test currents. (c) Current–voltage (I – V) characteristics of 5 nm thick \times 200 nm wide \times 30 μ m long Ba122:Co nanowire at various temperatures. (d) Temperature dependence of critical current density of the Ba122:Co nanowire. Inset: I – V loop characteristics of the Ba122:Co nanowire and hysteresis behavior at 10 K.

16 K, the J_c was 1.1×10^7 $A\,cm^{-2}$; even when the temperature reaches 20 K, the J_c still remains above 5.0×10^6 $A\,cm^{-2}$, demonstrating excellent current-carrying capabilities of the Ba122:Co nanowire. The inset of figure 6(d) shows I – V loop characteristics of Ba122:Co nanowire, which exhibits a voltage jump at a critical current (I_c) and a small hysteresis behavior, which is typical for long superconducting nanowire [37]. The difference between the critical current I_c and the hysteresis current I_h is about 20 μ A. It is unfortunate that the voltage switch effect in our nanowire from the superconducting to the normal state is weaker than previous reports [17], which may affect the output signal of SNSPD readout due to smaller voltage switch.

The I – V of Ba122:Co nanowires shows flux–flow type behaviors, which were also observed in the early $YBa_2Cu_3O_{7-\delta}$ nanowires [25]. However, with the improvement of film quality and nanowire processing technology, the I – V flux–flow phenomenon has been almost eliminated in the highly uniform $YBa_2Cu_3O_{7-\delta}$ and $La_{1.85}Sr_{0.15}CuO_4$ nanowires [4, 8]. Therefore, it is possible to eliminate the flux–flow of the Ba122:Co nanowire at low currents by adopting a more suitable process for Ba122:Co nanowires and improving the quality of Ba122:Co thin films. In addition, the characteristics of Ba122:Co

nanowire superconducting transition shows a high T_c , narrow ΔT_c and large J_c . In particular, the T_c of Ba122:Co nanowire reaching 20 K is comparable to MgB_2 nanowires [36, 38]. These results will certainly attract attention in the application of superconducting electronics and may open the door for developing Ba122:Co SNSPDs with higher operating temperatures, although in this case a new patterning process must be developed and the physical mechanism responsible for the I – V curve needs to be investigated.

Conclusions

For the first time, the 10 nm thick Ba122:Co films were successfully prepared by PLD. Furthermore, we succeeded in developing Ba122:Co nanowire fabrication processes and fabricated superconducting nanowires in 200 nm wide \times 30 μ m long on Ba122:Co films. The nanowires show $T_c^{zero} = 20$ K, $\Delta T_c = 2.5$ K and $J_c = 1.8 \times 10^7$ $A\,cm^{-2}$ at 10 K. Based on the current results, we believe that the ultra-thin Ba122:Co nanowires will attract interest in electronic applications, including SNSPDs.

Acknowledgments

The authors would like to express their thanks to Dr He Huang, Chao Yao and Chiheng Dong for many useful discussions. This work is partially supported by the National Natural Science Foundation of China (Grant Nos. 51320105015 and 51607174), the Beijing Municipal Science and Technology Commission (Grant No. Z141100004214002), the Bureau of Frontier Sciences and Education, Chinese Academy of Sciences (QYZDJ-SSW-JSC026) and the Beijing Training Project for the Leading Talents in S & T (Grant No. Z151100000315001).

ORCID iDs

Pusheng Yuan  <https://orcid.org/0000-0002-5074-7669>

References

- [1] Gol'tsman G, Okunev O, Chulkova G, Lipatov A, Semenov A, Smirnov K, Voronov B, Dzardanov A, Williams C and Sobolewski R 2001 *Appl. Phys. Lett.* **79** 705
- [2] Natarajan C, Tanner M and Hadfield R 2012 *Supercond. Sci. Technol.* **25** 063001
- [3] Shibata H, Takesue H, Honjo T, Akazaki T and Tokura Y 2010 *Appl. Phys. Lett.* **97** 212504
- [4] Shibata H, Kirigane N, Fukao K, Sakai D, Karimoto S and Yamamoto H 2017 *Supercond. Sci. Technol.* **30** 074001
- [5] Lyatti M, Savenko A and Poppe U 2016 *Supercond. Sci. Technol.* **29** 065017
- [6] Zhang C, Wang D, Liu Z-H, Zhang Y, Ma P, Feng Q, Wang Y and Gan Z 2015 *AIP Adv.* **5** 027139
- [7] Arpaia R, Ejrnaes M, Parlato L, Tafuri F, Cristiano R, Golubev D, Sobolewski R, Bauch T, Lombardi F and Pepe G 2015 *Physica C* **509** 16–21
- [8] Arpaia R, Golubev D, Baghdadi R, Ciano R, Dražić G, Orgiani P, Montemurro D, Bauch T and Lombardi F 2017 *Phys. Rev. B* **96** 064525
- [9] Ma Y 2012 *Supercond. Sci. Technol.* **25** 113001
- [10] Ma Y 2015 *Physica C* **516** 17–26
- [11] Hiramatsu H, Katase T, Kamiya T and Hosono H 2012 *J. Phys. Soc. Jpn.* **81** 011011
- [12] Seidel P 2011 *Supercond. Sci. Technol.* **24** 043001
- [13] Iida K, Hänisch J, Trommler S, Haindl S, Kurth F, Hühne R, Schultz L and Holzapfel B 2011 *Supercond. Sci. Technol.* **24** 125009
- [14] Bellingeri E, Pallecchi I, Buzio R, Gerbi A, Marrè D, Cimerle M, Tropeano M, Putti M, Palenzona A and Ferdeghini C 2010 *Appl. Phys. Lett.* **96** 102512
- [15] Yuan P, Xu Z, Ma Y, Sun Y and Tamegai T 2017 *IEEE Trans. Appl. Supercond.* **27** 7500105
- [16] Ge J, Liu Z, Liu C, Gao C, Qian D, Xue Q, Liu Y and Jia J 2015 *Nature Mater.* **14** 285–9
- [17] Rall D, Il'in K, Iida K, Haindl S, Kurth F, Thersleff T, Schultz L, Holzapfel B and Siegel M 2011 *Phys. Rev. B* **83** 134514
- [18] Döring S, Schmidt S, Schmidl F, Tympel V, Haindl S, Kurth F, Iida K, Mönch I, Holzapfel B and Seidel P 2012 *Supercond. Sci. Technol.* **25** 084020
- [19] Wu C, Chang W, Jeng J, Wang M, Li Y, Chang H and Wu M 2013 *Appl. Phys. Lett.* **102** 222602
- [20] Katase T, Hiramatsu H, Yanagi H, Kamiya T, Hirano M and Hosono H 2009 *Solid State Commun.* **149** 2121–4
- [21] Iida K, Hänisch J, Hühne R, Kurth F, Kitzun M, Haindl S, Werner J, Schultz L and Holzapfel B 2009 *Appl. Phys. Lett.* **95** 192501
- [22] Katase T, Hiramatsu H, Kamiya T and Hosono H 2010 *Appl. Phys. Express.* **3** 063101
- [23] Kurth F *et al* 2013 *Appl. Phys. Lett.* **102** 142601
- [24] Yuan P, Xu Z, Wang D, Zhang M, Li J and Ma Y 2017 *Supercond. Sci. Technol.* **30** 025001
- [25] Arpaia R, Ejrnaes M, Parlato L, Cristiano R, Arzeo M, Bauch T, Nawaz S, Tafuri F, Pepe G and Lombardi F 2014 *Supercond. Sci. Technol.* **27** 044027
- [26] Semenov A, Gol'tsman G and Sobolewska R 2002 *Supercond. Sci. Technol.* **15** R1–16
- [27] Ni N, Tillman M, Yan J, Kracher A, Hannahs S, Bud'ko S and Canfield P 2008 *Phys. Rev. B* **78** 214515
- [28] Wang Y, Plackowski T and Junod A 2001 *Physica C* **355** 179–93
- [29] Yuan P, Xu Z, Zhang H, Wang D, Ma Y, Zhang M and Li J 2015 *Supercond. Sci. Technol.* **28** 065009
- [30] Tsukada I *et al* 2011 *Appl. Phys. Express.* **4** 053101
- [31] Hänisch J *et al* 2015 *Sci. Rep.* **5** 17363
- [32] Tarantini C, Kametani F, Lee S, Jiang J, Weiss J D, Jaroszynski J, Hellstrom E E, Eom C B and Larbalestier D C 2014 *Sci. Rep.* **4** 7305
- [33] Takano S, Ueda S, Takeda S, Sugawara H and Naito M 2012 *Physica C* **475** 10–3
- [34] Lei Q *et al* 2014 *Supercond. Sci. Technol.* **27** 115010
- [35] Nappi C, Camerlingo C, Enrico E, Bellingeri E, Braccini V, Ferdeghini C and Sarnelli E 2017 *Sci. Rep.* **7** 4115
- [36] Shimakage H and Zhen W 2013 *IEEE Trans. Appl. Supercond.* **23** 2200104
- [37] Shibata H 2014 *Appl. Phys. Express.* **7** 103101
- [38] Shibata H, Maruyama T, Akazaki T, Takesue H, Honjo T and Tokura Y 2008 *Physica C* **468** 1992–4